J. Plasma Physics (2012), vol. 78, part 2, pp. 165–174. © Cambridge University Press 2011
doi:10.1017/S0022377811000535

Electron drift caused by rf field gradient creates many plasma phenomena: An attempt to distinguish the cause and the effect

C. L. XAPLANTERIS[1,2], E. D. FILIPPAKI[1], I. S. MISTAKIDIS[2] and L. C. XAPLANTERIS[3]

[1]Plasma Physics Laboratory, IMS, NCSR 'Demokritos', Athens, Greece
[2]Hellenic Military Academy, Vari Attica, Greece
[3]Faculty of Physics, School of Sciences, National and Kapodistrian University of Athens, Panepistimiopolis, 15771 Ilissia, Athens, Greece
(cxaplanteris@yahoo.com)

(Received 23 August 2011; revised 14 October 2011; accepted 13 November 2011; first published online 12 December 2011)

Abstract. Many experimental data along with their theoretical interpretations on the rf low-temperature cylindrical plasma have been issued until today. Our Laboratory has contributed to that research by publishing results and interpretative mathematical models. With the present paper, two issues are being examined; firstly, the estimation of electron drift caused by the rf field gradient, which is the initial reason for the plasma behaviour, and secondly, many new experimental results, especially the electron-neutral collision frequency effect on the other plasma parameters and quantities. Up till now, only the plasma steady state was taken into consideration when a theoretical elaboration was carried out, regardless of the cause and the effect. This indicates the plasma's complicated and chaotic configuration and the need to simplify the problem. In the present work, a classification about the causality of the phenomena is attempted; the rf field gradient electron drift is proved to be the initial cause.

1. Introduction

Although the plasma as a physical state has been studied by the scientific community during the last decades of the 20th century only (Drummond 1961; Arzimovich 1965; Spitzer 1967), enough bibliography has been gathered concerning the plasma and its phenomena (Krall and Trivelpiece 1973; Lieberman and Lichtenberg 1994; Wesson 1997). Waves of any kind that are developed because of the increasing plasma loss have been systematically overhauled. Among these waves, there are the electrostatic ion waves (D'Angelo 1963; Chen 1964) and the drift waves which propagate at low frequencies and are caused on various gradients (D'Angelo and Motley 1963; Hendel et al. 1967; Ellis et al. 1980; Marden-Marshhall et al. 1986; Lakhina and Shukla 1987; Shukla et al. 1995; Vranjes et al. 2004). Extensive research has been done on the drift waves of the quiet fully ionized gas caused by the density gradient. Drift waves may rise in weakly ionized plasma as well, if we consider that the waves helically propagate. There is a small component k_z of the wave vector, which is indispensable for the growth rate existence of the collision mechanism between electrons and neutral atoms (resistive instability).

The plasma production method is also of important significance. The rf-produced plasma is a method which has remarkable advantages in comparison with other production methods. The possibility of having electrodeless discharge is one of them. When one rf-produced discharge is created in a constant magnetic field, these advantages grow in numbers. By using the electron–cyclotron resonance, the produced plasma has higher energy than the one that occurs without magnetic field. Moreover, the discharge lights up easily (Krall and Trivelpiece 1973; Wesson 1997).

Such an rf-produced plasma with magnetic confinement was established in the Plasma Physics Laboratory of NCSR 'Demokritos' and many results were observed and studied during the last two decades (Xaplanteris 1987, 2009, 2011; Xaplanteris and Filippaki 2011). By having a coaxial geometrical symmetry of the cavity, we always had the ability to give the appropriate interpretation on the phenomena in a determinative way. All the theoretical elaborations on the measurements of the plasma steady state have been studied. But, as the plasma quantities are numerous and bound together, we are not able to know what is the cause and what is the result, and the state becomes chaotic (Koepke et al. 1996; Klinger 1998; Block et al. 2001). In the present paper, it is proved that the rf-electric potential gradient gives an azimuthal drift velocity especially to electrons (ions are far away from resonance). This proof is based on the Microwave Transmission Theory (Moreno 1948; Heald and Wharton 1965), and leads to the electron rf-drift without any presupposition. So, as the electron rf-drift rises, a creation of a chronological-causality series of plasma quantities is attempted. The mapping of the

risen plasma electrostatic waves was another intention of this work, as well as the gas mixture plasma study.

The paper is organized as follows: in Sec. 2, the purpose and the experimental device are given. In Sec. 3, the experimental data presentation is included. The mathematical elaboration is presented in Sec. 4 and Sec. 5 contains the complete interpretation of the experimental results. Finally, the detailed rf-drift elaboration is presented in the Appendix.

2. Experimental part

2.1. Experiment purpose

As is well known, plasma is a complex state, as it contains a large number of degrees of freedom, which makes it virtually very difficult to achieve the defined target by designing an experiment for laboratory plasma production. In very few cases, experimental plasma behaves in the way that was predicted by the plan. So, for a sufficient limitation of the discrepancy between the predicted and actual outcome of the experiment, a quiet Argon plasma with the simple and symmetric geometry has to be designed for the semi Q-machine. Beyond the secondary observations and phenomena which have arisen, the main idea was to study the role of the rf electrical field on the other plasma parameters, as well as to find the priority and cohesion of plasma phenomena and physical quantities. These phenomena are impossible to be distinguished on the plasma steady state. Since the symmetric cylindrical geometry is the most convenient mathematically, the following experimental apparatus was used.

2.2. Experimental set-up

With the purpose of producing quiet plasma using the simplest geometry, a cylindrical cavity has to be chosen. Moreover, the complete symmetry of the plasma column has been sought to make the theoretical elaboration convenient and understandable. In this way, a cylinder made of steady steel with 50 cm in length and 6 cm in the internal diameter, is enclosed by two circular metallic disks. A steady steel antenna 40 cm in length and 0.6 cm in diameter is fastened on one base's centre, so as to form along with the cylinder (external conductor) a coaxial line. The rf wavy power is entered into the cavity through this antenna. Two portals on the cylinder's curved surface are antidiametrically opened, one for the gases input and the other is connected to the pump. The first one is equipped with two valves, so that two gases (Argon and Helium) or their mixture can be used.

A disk probe is radially moving around its axis in favour of the azimuthal drift current. Other Langmuir electrostatic probes are moving radially and parallel to the tube axis, since a five-probe array is checking up the plasma column azimuthally. A drawing of the apparatus is given in Fig. 1.

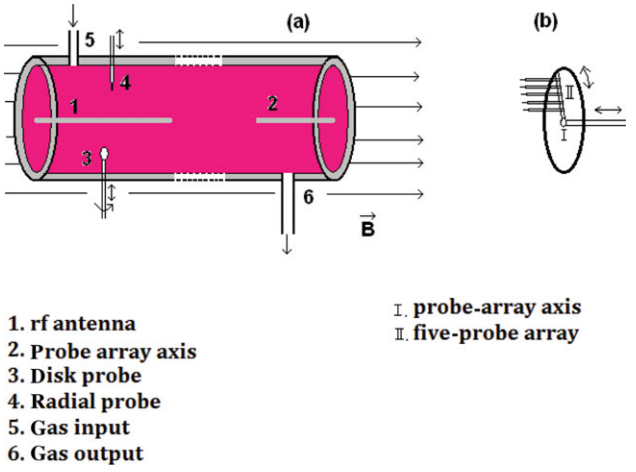

Figure 1. (Colour online) (a) The cavity outline at the external magnetic field. (b) The probe array system.

Table 1. Plasma parameters ranging values.

Parameters	Minimum value	Maximum value
Argon pressure p	0.001 Pa	0.1 Pa
Argon number density, n_g	$2 \times 10^{15}\,\mathrm{m}^{-3}$	$2 \times 10^{17}\,\mathrm{m}^{-3}$
Magnetic field intensity, B	10 mT	200 mT
Microwaves' power, P	20 Watt	120 Watt
Frequency of the rf power (standard value)	2.45 GHz	
Electron density, n_0	$2 \times 10^{15}\,\mathrm{m}^{-3}$	$4.6 \times 10^{15}\,\mathrm{m}^{-3}$
Electron temperature, T_e	1.5 eV	10 eV
Ion temperature, T_i	0.025 eV	0.048 eV
Ionization rate	0.1%	90%
Electron drift velocity, u_e	$1 \times 10^4\,\mathrm{m/s}$	$1.7 \times 10^4\,\mathrm{m/s}$
Electron-neutral collision frequency, ν_e	$1.2 \times 10^7\,\mathrm{s}^{-1}$	$3 \times 10^9\,\mathrm{s}^{-1}$

3. Measurements and results

Just as it was shown in previous publications of our Laboratory (Xaplanteris 1987, 2009, 2011; Xaplanteris and Filippaki 2011), an Argon plasma may light within a large value range of the external plasma parameters (gas pressure p, rf-field power P, magnetic field stress B). Those large value ranges lead to an extension of plasma parameters range as well. Such plasma parameters are the plasma density, plasma temperature, dc electrical potential, collision frequency, etc. It must be noted that the Helium plasma is produced within closer parameter values than the Argon plasma. The range of plasma parameter values is listed in Table 1; the minimum and maximum value of each parameter is visible.

3.1. Waves mapping

Among the first observation was the fact that the plasma may easily light up when the magnetic field $\vec{B}$ slightly varies around the value $B_{res} = 84,5\,\mathrm{mT}$, which corresponds to the electron–cyclotron resonance with the external rf-field frequency. It must be noted that plasma originates only from the electron–cyclotron resonance, although it can afterwards be maintained far away from

https://doi.org/10.1017/S0022377811000535 Published online by Cambridge University Press

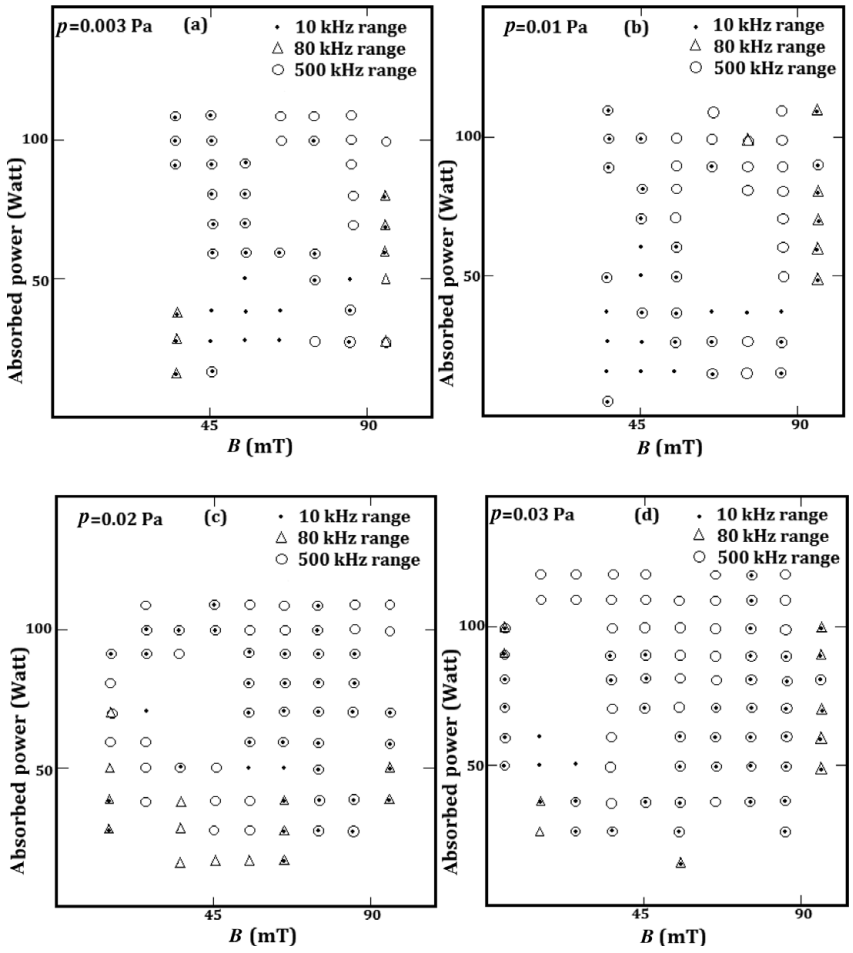

Figure 2. Wave rising ranges.

it. The opposite process for plasma to originate far away from resonance has never been observed.

Another important observation was the persistent and clear appearance of different kinds of plasma waves. These waves have been classified in three frequency ranges of 10 kHz, 80 kHz and 500 kHz. Each fundamental was always accompanied by its higher harmonics.

As the waves are sensitive from the external plasma parameter point of view, they have been completely mapped for four pressure values. Figure 2 shows the range of the three basic parameters (gas pressure, magnetic field stress and absorbed rf power), that is where the plasma waves rise or disappear.

The absence of waves is shown with an almost rectangular shape, which moves for lower magnetic field stress values as the gas pressure increases. The results of Fig. 2 are the same, regardless of the probe that was used; only the wave amplitude is different on each probe, a fact that indicates that the wave development is affected by the probe's position into the cavity.

3.2. Pressure influence on plasma temperature and density

After the experimental definition of the external parameters' range where the plasma is produced, the plasma parameters (electron temperature T_e, plasma density n_0, dc electric field $\vec{E}$, etc.) were measured. So, the electron temperature and plasma number density dependence on the gas pressure for different absorbed power values are listed in Table 2 and depicted in Figs. 3, 4.

Figure 3 shows that the electron temperature decreases as the gas pressure increases at low pressure values, while it remains the same as the gas pressure moves at high values.

At the same time, the estimation of the plasma density was carried out, as the gas pressure varied. The measured values are also shown in Table 2, while the drawing is separated in Fig. 4 for clarity.

It must be noted that the plasma density is increasing with the gas pressure until it reaches a definite pressure value p_c, and then it begins to decrease.

3.3. Study on the radial dc electric field

It is expected that the electron drift velocity strongly affects the charge separation and a dc electric field can be produced. So, the dc electric potential must be researched and studied in all directions, and especially along the cylinder radius. The measurement was performed by the radially moving electrostatic probe, properly placed near the antenna where the plasma is produced. Gas pressure and magnetic field stress

https://doi.org/10.1017/S0022377811000535 Published online by Cambridge University Press

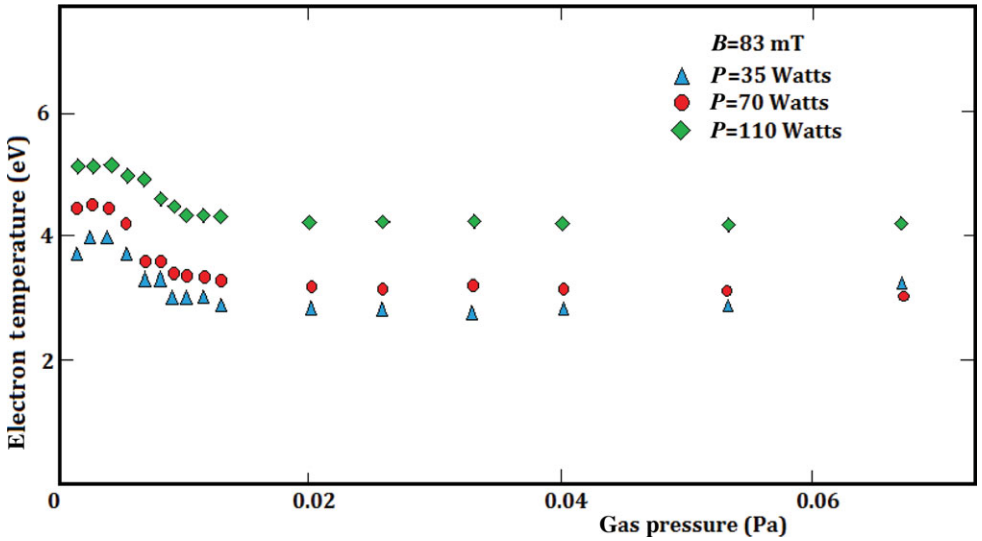

Figure 3. (Colour online) The electron temperature versus the gas pressure.

Table 2. Gas pressure influence on electron temperature and plasma density.

P	$W = 35$ Watt	$W = 35$ Watt	$W = 70$ Watt	$W = 70$ Watt	$W = 110$ Watt	$W = 110$ Watt
Pa	T_e(eV)	$n_0(\times 10^{15}\,\mathrm{m}^{-3})$	T_e(eV)	$n_0(\times 10^{15}\,\mathrm{m}^{-3})$	T_e(eV)	$n_0(\times 10^{15}\,\mathrm{m}^{-3})$
0.0013	3.58	1.10	4.20	2.00	5.32	2.81
0.0027	3.85	1.15	4.20	2.10	5.30	2.88
0.0040	3.74	1.20	4.12	2.15	5.30	2.92
0.0053	3.74	1.22	4.03	2.32	5.20	2.91
0.0067	3.75	1.23	3.70	2.38	5.03	2.99
0.0080	3.15	1.26	3.75	2.41	4.70	3.11
0.0093	3.04	1.28	3.55	2.42	4.64	3.13
0.0107	3.04	1.28	3.50	2.43	4.52	3.11
0.0120	3.10	1.25	3.52	2.40	4.50	3.10
0.0133	2.89	1.23	3.45	2.40	4.33	3.03
0.0200	2.74	1.20	3.36	2.37	4.29	3.00
0.0267	2.66	1.18	3.28	2.30	4.27	2.95
0.0333	2.49	1.16	3.31	2.29	4.30	2.90
0.0400	2.57	1.15	3.23	2.26	4.25	2.83
0.0533	2.62	1.12	3.20	2.20	4.21	2.75
0.0667	3.32	0.9	3.19	2.03	4.20	2.71

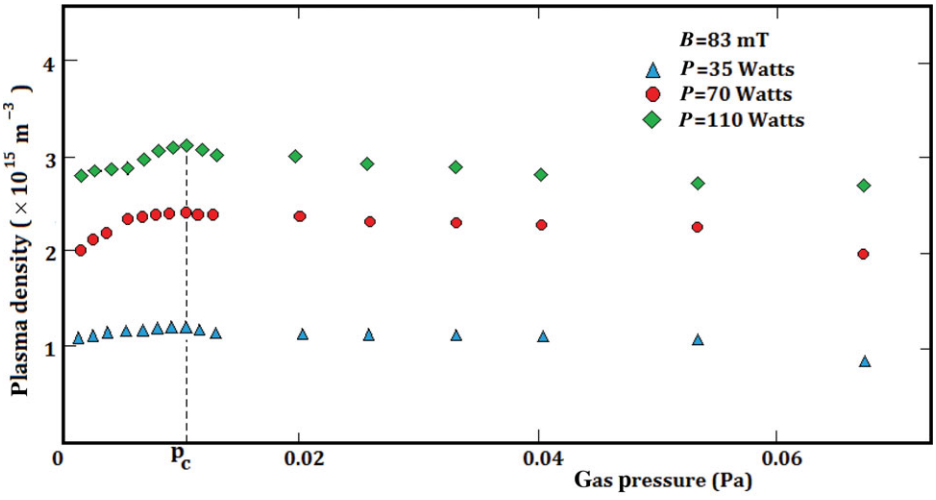

Figure 4. (Colour online) The plasma density versus the gas pressure.

https://doi.org/10.1017/S0022377811000535 Published online by Cambridge University Press

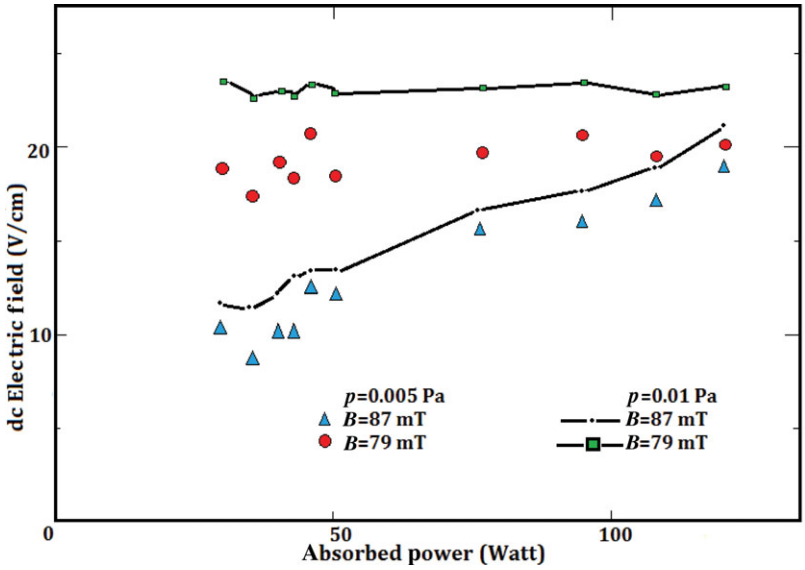

Figure 5. (Color online) The dc electric field versus the power above and under the electron cyclotron resonance.

remained at the same value, while the absorbed power varied. The measured values are depicted in Fig. 5; as the experiment was repeated for magnetic field intensity above and below the electron–cyclotron resonance, it must be noted that, in the first case, the dc electric field grew along with the absorbed power, whereas in the second one it remained at the same value.

As the experiment was repeated in the same way but at a higher gas pressure ($p = 0.01\,Pa$), the dc electric field behaved similarly as before, except for the electron number density, the values of which increased. This result confirms the previous one and both of them are presented in Fig. 5.

3.4. *Pressure influence on wave frequency and amplitude*

The gas pressure influence on the wave is shown in Fig. 6, by presenting four wave spectra.

It is evident that the increase of the pressure causes a perceptible decrease of the wave frequency and amplitude. The complete series of measurements for three absorbed power values and for magnetic field intensity above the electron–cyclotron resonance ($B = 87\,\mathrm{mT}$) is listed in Table 3 and is depicted in Fig. 7.

The complete series of measurements have been repeated for the magnetic field below the upper hybrid resonance ($B = 79\,\mathrm{mT}$). As the results were similar to the previous one, they seemed not important to be stated again.

3.5. *Gas mixture plasma*

In the experimental device description, the ability to produce Helium plasma was mentioned. So, both the pure Argon plasma and the mixed Argon–Helium plasma were examined. The discharge gas was firstly pure Argon; during the experiment, the gas was gradually enhanced with Helium while Argon was gradually decreased, till the gas mixture ended in pure Helium.

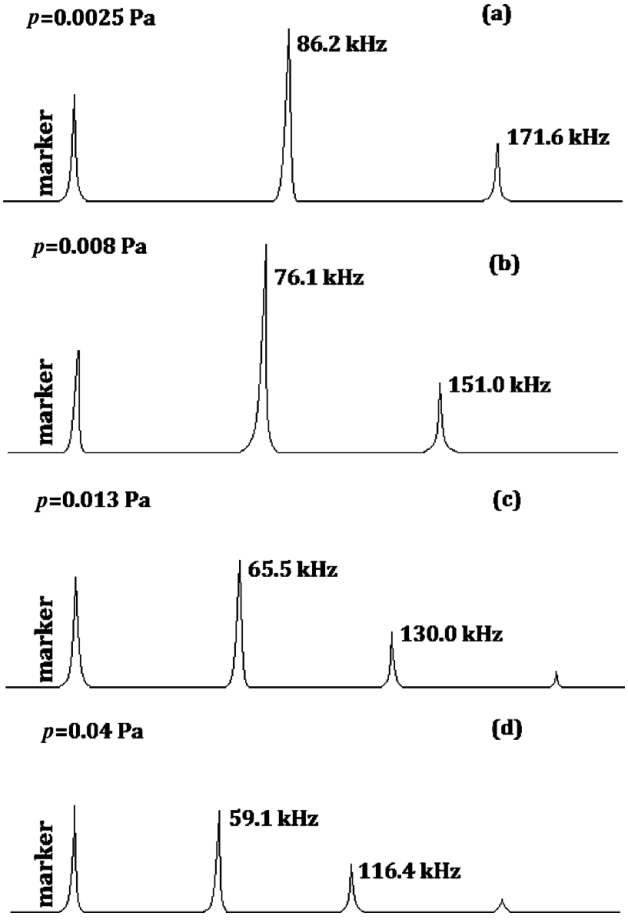

Figure 6. Four wave spectra for different pressure values.

The results for the pure Helium plasma are the following: the low-frequency waves appeared. These waves obey the middle range (80 kHz) dispersion relation and they have a smaller value at the fundamental frequency ($l = 1$), as well as at the higher harmonics. Figure 8 shows a typical spectrum of low-frequency waves produced in the Helium plasma.

https://doi.org/10.1017/S0022377811000535 Published online by Cambridge University Press

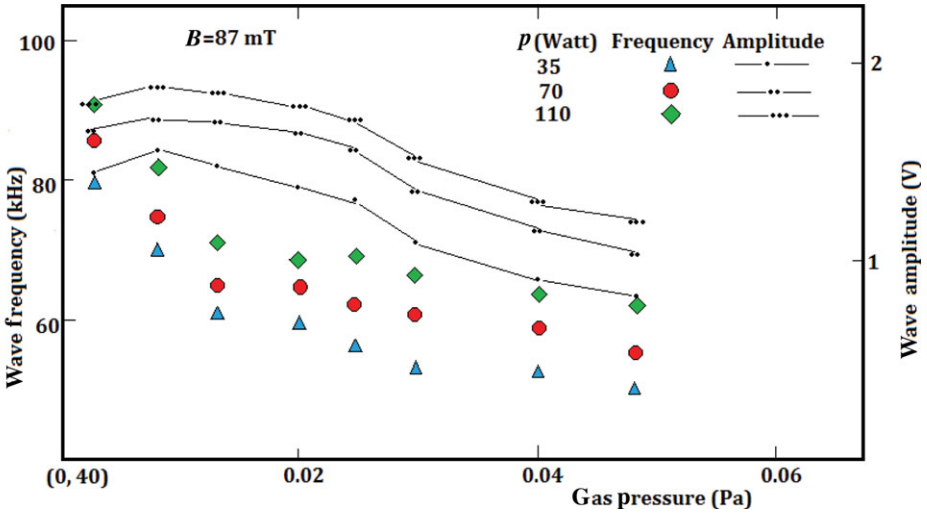

Figure 7. (Colour online) Wave frequency and wave amplitude for three power values.

Table 3. Wave frequency and amplitude as the gas pressure changes.

	$P = 35$ Watt		$P = 70$ Watt		$P = 110$ Watt	
Pressure (Pa)	Wave frequency (kHz)	Wave amplitude (V)	Wave frequency (kHz)	Wave amplitude (V)	Wave frequency (kHz)	Wave amplitude (V)
0.0025	80.0	1.42	86.2	1.64	91.5	1.79
0.008	70.5	1.55	76.1	1.71	83.0	1.87
0.013	61.2	1.48	65.5	1.70	71.8	1.84
0.020	60.0	1.37	64.8	1.64	68.7	1.77
0.025	57.3	1.31	62.1	1.56	69.7	1.70
0.030	54.6	1.10	61.3	1.35	67.1	1.51
0.040	53.4	0.90	59.1	1.15	63.8	1.30
0.048	51.0	0.83	56.6	1.03	62.4	1.19

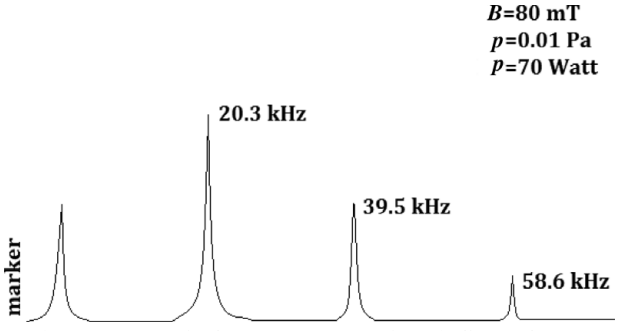

Figure 8. A typical wave spectrum in a helium plasma.

Moreover, it was observed that the maximum wave amplitude appears near the antenna, in comparison with the Argon plasma wave.

The wave frequency of the mixture of Argon–Helium plasma decreases with the rate of Helium concentration. In Fig. 9, four spectra are presented with the aim to show the influence of the mixture percentage on the wave frequency.

Starting from pure Argon plasma (Fig. 9(a)), we end up with pure Helium plasma (Fig. 9(d)). In the absence of suitable devices for measuring gas participation, Fig. 9(b) is characterized as 'low percentage of Helium' and Fig. 9(c) as 'high Helium percentage'.

4. Theoretical model

If a charged particle (q, m) is present in a homogeneous magnetic field $\vec{B}$ and rf electric field $\vec{E}(\vec{r}, t)$, then the particle motion is described by the following equation:

$$\frac{\partial \vec{V}}{\partial t} = \frac{q}{m} \cdot \vec{E}(\vec{r}, t) + \omega_c \vec{V} x \vec{z} - v \vec{V}, \qquad (1)$$

where $\vec{r}$ is the particle distance from the cavity' axis, v is the collision frequency between charged particles and neutrals and $\omega_c = \frac{qB}{m}$ the cyclotron frequency.

It is considered that the rf electric field stress for the TEM mode (Moreno 1948) into a coaxial line is

$$\vec{e}(\vec{r}, t) = E(\rho, t)\hat{e}_\rho = \frac{377 I_0}{2\pi\sqrt{\varepsilon_\perp \cdot \rho}} \cdot \sin \omega_R t \cdot \hat{e}_\rho \qquad (2)$$

with

$$\varepsilon_\perp = \frac{(\omega_r^2 - v^2 - \omega_c^2)^2 + 4v^2\omega_R^2 - \omega_P^2(\omega_R^2 + v^2 - \omega_c^2)}{(\omega_R^2 - v^2 - \omega_c^2)^2 + 4v^2\omega_R^2},$$

which is the plasma perpendicular electric constant (Heald and Wharton 1965).

By the electric field expansion around the centre of the cycloid orbit and the separation of the zero- and first-order perturbation, we get the azimuthal drift velocity

https://doi.org/10.1017/S0022377811000535 Published online by Cambridge University Press

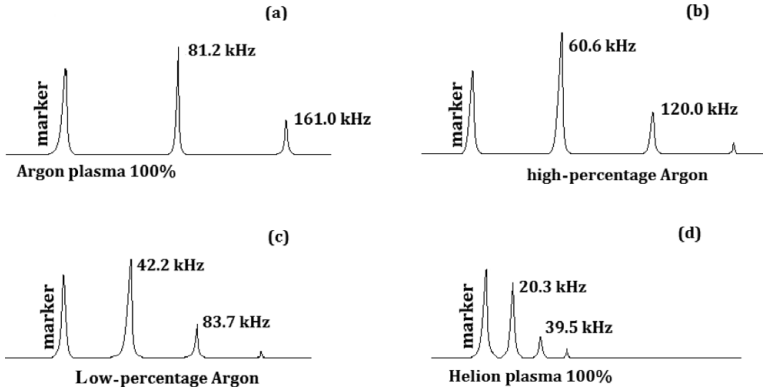

Figure 9. Wave spectra for different percentage of argon-helium mixture.

as

$$u_\theta = \frac{\omega_c}{\omega_c^2 + v^2} \frac{E_0^2}{2R^3} \frac{\omega_c^2 + v^2 - \omega_R^2}{(\omega_R^2 - v^2 - \omega_c^2)^2 + 4v^2\omega_R^2 - \omega_P^2(\omega_R^2 + v^2 - \omega_c^2)}, \tag{3}$$

where

$$E_0 = \frac{377q \cdot I_0}{2\pi m}.$$

The radial drift velocity is

$$u_\rho = -\frac{v}{\omega_c} u_\theta, \tag{4}$$

which has a powerful influence due to the collision frequency.

When the plasma is considered as collisionless, (3) is simplified as follows:

$$u_\theta = -\frac{E_0^2}{2R^3\omega_c} \frac{1}{\omega_R^2 - \omega_c^2 - \omega_p^2}. \tag{5}$$

For the given magnetic field stress (maximum value 2000 mT), it is impossible to have the ion–cyclotron resonance; as (5) shows, the azimuthal ion drift is very limited. On the contrary, the electron–cyclotron is a presupposition for the plasma to be lit and as $\omega_R \cong \omega_{ce}$, the electron drift velocity can temporarily take big values. In fact, the collisions limit the drift velocity even around the resonance.

Due to the collision mechanism, a radial drift velocity for the electrons exists and in accordance with (4) it is coupled to the azimuthal velocity. This radial drift velocity appears to be responsible for the radial dc electric field production, as, when the first quantity changes direction, the second one changes configuration, as justified below.

5. Experimental data interpretation

The basic purpose of the experiment was the chronicle arrangement of the physical phenomena, the cause and the result. As the transition time is very limited, only the measurements on the steady state can be described while the phenomena on the transitive state are hidden. In the transitive state, the optical observation can be in use, which has the ability to be recorded on video. By using the optical observation, we assured that the wave is moving from a higher frequency value and it is established in the low final one f_0. The higher wave frequency requires a bigger electron drift velocity, which can be produced by the rf electric field at the electron–cyclotron resonance, as (5) shows. It was experimentally assured that the plasma lights up only at the electron–cyclotron resonance, and then it exists far away from this resonance. The opposite process does not occur: the plasma cannot light up away from the resonance. The same conclusion is theoretically verified, as was shown in Sec. 4 (in detail in the Appendix), the rf electric drift production does not require any presupposition, apart from the rf field presence. By the above consideration, the following succession is unavoidable: firstly, a big electron rf drift is produced near the electron–cyclotron resonance. This big rf electron drift, due to the radial drift component $u_\rho = -\frac{v}{\omega_c} u_\theta$ separates the charge and the dc electric field is produced. The dc electric field creates in its turn an azimuthal drift for electrons and ions and the low-frequency waves are developed. The electrostatic waves trap the free electrons, reduce their velocity and steady state is established.

5.1. *Waves mapping*

The waves mapping shows absence of waves which are moving towards lower magnetic field values as the gas pressure is increasing. Although the causes were not determined exactly, it is evident that in these range values of B, P and p, the wave growth rate does not exist, because the rf electron drift and the electron drift from the density gradient are opposite.

5.2. *Pressure influence on plasma temperature and density*

As we can see in Fig. 3, the increase in gas pressure leads to the electron temperature diminution. This result can be explained by the following consideration. If the absorbed power remains constant, the gas ionization increases until a definite pressure value p_c is reached (after that, gas ionization decrease occurs); the amount

https://doi.org/10.1017/S0022377811000535 Published online by Cambridge University Press

of microwave energy, which is required for gas ionization, is large and the remaining amount for the electron kinetic energy increase is low. In addition, the pressure increase causes the increase of the collision frequency v_{en} while the energy transfer from electrons to neutrals reduces the electron temperature. When the pressure becomes high, gas ionization is reduced and the microwave energy, which is disposed of for the electron kinetic energy, is higher. The increase of the electron temperature T_e is balanced by the energy loss due to the collision frequency, and results in temperature stability. Figure 4 shows that gas ionization firstly increases as the pressure increases to a definite value p_c, and then reduces due to the electron collision frequency increase. It must be noted that between the absorbed power and electron density, the expected quasi-analogy exists.

5.3. Studies on the radial dc electric field

In Fig. 5, the dc electric field is shown as the absorbed power varies. Measurements were taken near the antenna where the plasma is produced for two magnetic field values, above and under the electron–cyclotron resonance. We must take into consideration two factors, which contribute to dc electric field formation: the perpendicular electron diffusion and the electron moving due to the radial rf electric drift-up. When the magnetic field is $B = 79\,\mathrm{mT}$, which is under upper hybrid resonance, the electrons radially drift with $u_\rho > 0$ from the antenna to the external conductor. In the plasma diffusion, as Spitzer (1967) showed, the magnetic field presence causes the ions to diffuse more quickly than the electrons and a superabundance of electrons is formed. The positive drift velocity of electrons has the tendency to neutralize the superabundance of electrons and the plasma comes into the neutrality state. As the Poisson law shows, $\nabla \cdot \vec{E} = \frac{e \cdot \Delta \vec{n}}{\varepsilon_0}$, the charge difference $\Delta \vec{n}$ has the tendency of becoming zero and, consequently, the electric field E must be constant. By increasing the absorbed power, the two factors are increased together, in order to secure the plasma neutrality and consequently the electric field stability.

For the magnetic field $B = 86\,\mathrm{mT}$, which is above the hybrid resonance, the drift velocity is negative and the electrons are moving from the external conductor to the antenna. In this case, the diffusion and the electron radial drift are acting the same way, so that the total electric field E grows along with the absorbed power.

If the experiment is repeated for higher gas pressure, the same phenomena will appear. The only difference as the pressure increases is that the measured dc electric field is slightly higher. This is understandable because an increase of the pressure leads to the increase of the electron density as well. The electron density affects both the collision frequency and the diffusion in the same way, and finally, the dc electric field.

5.4. Pressure influence on wave frequency and amplitude

The general result of the present experiment is the following: the increase of the gas pressure always causes i) the wave frequency to decrease and ii) for the wave amplitude to decrease below the critical value $p_{c,}$ and to decrease for higher pressure values. The understanding is easy if we take into consideration a) the electron number density change versus the gas pressure (Fig. 4); the plasma density n_0 increases until the critical value p_c and afterwards it decreases as the pressure p becomes higher, b) the collision frequency v_e is proportional to the plasma density and it follows its changes with the pressure and c) for the wave range of 80 kHz, the dispersion relation is valid (see (5) of Xaplanteris 2009)

$$\omega \cong k u_e + j v_e \frac{\omega_{pe}^2}{\omega_{pi}^2} \cdot \frac{k^2(u^2 - C_s^2) - \omega_{ci}^2}{\omega_{ce}^2}. \tag{6}$$

From (6), it is evident that the growth rate and consequently the wave amplitude follow the collision frequency changes in the same way, as Fig. 7 thus showing that d) the electron trapping, which strongly affects the electron drift velocity u_e, is directly influenced by the wave amplitude. As (6) indicates, the wave frequency ω is proportional to u_θ, which is affected by the gas pressure, in accordance with the above considerations.

The experiment was repeated for three absorbed power values and the results, which are shown in Fig. 7, can be interpreted as follows: in an rf field discharge where an external magnetic field is present, the ion production power S (ions which are produced per unit of volume and time), is given by the equation

$$S = \frac{2aAS^+}{\varepsilon} e^{-2a\times}, \tag{7}$$

where A is the absorption factor, S^+ the intensity of the entered power, $\times$ the thickness and ε the average needed energy for the production of a couple of ions. That means that the plasma density and, consequently, the collision frequency, is proportional to the absorbed power. The collision frequency affects the growth rate of the wave (see (6)), and the result is the increase in electron trapping. This is accompanied by the azimuthal electron drift increase and an increase in the wave frequency as well.

5.5. Gas mixture plasma

Although some observations about the gas mixture plasma were given in Sec. 3.5, an effort to give a physical interpretation of the results is also made in this paragraph. As the Helium ion is almost 10 times smaller than the Argon ion, the rf azimuthal drift for Helium ions cannot be neglected. From this point of view, the total azimuthal ion drift appears to be strengthened, whereas the radial drift becomes smaller. The charged particles separation gives a small dc electrical field, which produces a little azimuthal drift. Perhaps the Helium ions, lighter as they are, are trapped by the wave and so the total trapped charge is reduced. The influence of the

https://doi.org/10.1017/S0022377811000535 Published online by Cambridge University Press

Helium ion fraction on the wave frequency decrease is shown in Fig. 9. In this way, the confirmation that the decrease of the frequency is caused by the Helium ion participation, is obtained.

The study of the gas mixture plasma has not been completed yet, and this remaining part of the research may be the object of the following work.

Acknowledgements

The authors wish to thank Dr A. J. Anastassiades for his valuable help in theoretical, as well as, in experimental subjects. They are also grateful to Dr Y. Bassiakos, Dr K. Theodorakopoulou and other members of the Plasma Laboratory of NCSR 'Demokritos' for their assistance in various ways. Many thanks to the colleagues-Physicists at the Hellenic Military Academy for their assistance on simulation issues. Especially Professor of English Language Laki Dina for her offer to proofread this study.

Appendix: Electron drift due to rf power finding

Momentum equation for a charged particle into a homogeneous magnetic field B and a high- frequency radio wave is written as:

$$m\frac{\partial \vec{V}}{\partial t} = q \cdot \vec{E}(\vec{r},t) + q \cdot \vec{V} x \vec{B} - vm\vec{V}, \qquad (A\,1)$$

where $\vec{r}$ is the particle distance from the axis z, $\vec{V}$ the particle velocity and v the collision frequency between charged particles and neutrals.

Taking into consideration that the cyclotron frequency is $\omega_c = \frac{qB}{m}$, the above equation becomes

$$\frac{\partial \vec{V}}{\partial t} = \frac{q}{m} \cdot \vec{E}(\vec{r},t) + \omega_c \vec{V} x \vec{z} - v\vec{V}. \qquad (A\,2)$$

The rf field intensity for the TEM mode into a coaxial line along z-axis is taken (Moreno 1948) as

$$\vec{e}(\vec{r},t) = E(\rho,t)\hat{e}_\rho = \frac{377 I_0}{2\pi\sqrt{\varepsilon_\perp \cdot \rho}} \cdot \sin\omega_R t \cdot \hat{e}_\rho, \qquad (A\,3)$$

where ρ is the particle distance from tube axis, I_0 is the line current amplitude in amperes, ω_R the radio frequency and $\varepsilon_\perp$ is the perpendicular electrical constant which is given by the relation (Heald and Wharton 1965)

$$\varepsilon_\perp = 1 - \frac{\omega_p^2(\omega_R^2 + v^2 - \omega_c^2)}{(\omega_R^2 - v^2 - \omega_c^2)^2 + 4v^2\omega_R^2} \qquad (A\,4)$$

with ω_p being the plasma frequency which is $\omega_p^2 = \frac{n_0 e^2}{m\varepsilon_0}$ and n_0 is the plasma number density. If in (A3), E_0 is replaced by

$$E_0 = \frac{377 q \cdot I_0}{2\pi m},$$

then (A2) is written as

$$\frac{\partial \vec{V}}{\partial t} = \frac{E_0}{\rho\sqrt{\varepsilon_\perp}} \cdot \sin\omega_R t \cdot \hat{e}_\rho + \omega_c \vec{V} x \hat{e}_z - v\vec{V}. \qquad (A\,5)$$

Due to the radial gradient of the rf field $E(\rho,t)$, the charged particles on cycloid orbits are moved. Considering one period of cycloid motion, the electrical field E may be expanded around the centre of the orbit

$$\vec{E}(\rho,t) = \vec{E}(R,t) + \frac{\partial \vec{E}}{\partial \rho}\Big|_R \chi_\rho = E(R,t)\hat{e}_\rho - E(R,t)\frac{\chi_0}{R}\hat{e}_\rho$$

and then (A5) becomes:

$$\frac{\partial \vec{V}}{\partial t} = \frac{E_0}{R\sqrt{\varepsilon_\perp}} \cdot \sin\omega_R t \cdot \hat{e}_\rho - \frac{x_0}{R} \cdot \frac{E_0}{r\sqrt{\varepsilon_\perp}} \cdot \sin\omega_R t \cdot \hat{e}_\rho + \omega_c \vec{V} x \hat{e}_z - v\vec{V}, \qquad (A\,6)$$

where $\vec{R}$ is the position vector of the orbit centre and $\vec{\chi}$ the position vector of the particle from the orbit centre.

By omitting the first-order component, the remaining equation leads to a zero-order solution

$$\frac{\partial \vec{V}^0}{\partial t} = \frac{E_0}{R\sqrt{\varepsilon_\perp}} \cdot \sin\omega_R t \cdot \hat{e}_\rho + \omega_c \vec{V}^0 x \hat{e}_z - v\vec{V}^0. \qquad (A\,7)$$

Separating (A7) along the radial and azimuthal directions, we take

$$\frac{\partial V_\rho^0}{\partial t} = \frac{E_0}{R\sqrt{\varepsilon_\perp}} \cdot \sin\omega_R t. + \omega_c V_\theta^0 - v V_\rho^0,$$

$$\frac{\partial V_\theta^0}{\partial t} = -\omega_c V_\rho^0 - v V_\theta^0.$$

A combination of the last two relations given above leads to the differential equation for V_ρ^0

$$\frac{\partial^2 V_\rho^0}{\partial t^2} + 2v\frac{\partial V_\rho^0}{\partial t} + (\omega_c^2 + v^{2)})V_\rho^0 = \frac{E_0}{\sqrt{\varepsilon_\perp} \cdot R}\omega_R \cos\omega_R t + \frac{E_0}{\sqrt{\varepsilon_\perp} \cdot R} v \cdot \sin\omega_R t. \qquad (A\,8)$$

A solution of the following form is sought:

$$V_\rho^0 = a\cos\,\omega_R t + b\sin\,\omega_R t,$$

where a and b are determinable factors.

With substitution of the proposed solution into (A8) and separation of the trigonometric terms, we end up with the algebraic system.

$$a(\omega_c^2 + v^2 - \omega_R^2) + 2v\omega_R b = \frac{E_0}{\sqrt{\varepsilon_\perp} \cdot R}\omega_R \cdot -2v\omega_R a$$

$$+ (\omega_c^2 + v^2 - \omega_R^2)b = \frac{E_0}{\sqrt{\varepsilon_\perp} \cdot R} v$$

from which the factors' value is estimated as

$$a = \frac{E_0}{\sqrt{\varepsilon_\perp} \cdot R}\omega_R \frac{\omega_c^2 - v^2 - \omega_R^2}{(\omega_c^2 + v^2 - \omega_R^2)^2 + 4v^2\omega_R^2},$$

$$b = \frac{E_0}{\sqrt{\varepsilon_\perp} \cdot R} v_R \frac{\omega_c^2 + v^2 + \omega_R^2}{(\omega_c^2 + v^2 - \omega_R^2)^2 + 4v^2\omega_R^2}. \qquad (A\,9)$$

https://doi.org/10.1017/S0022377811000535 Published online by Cambridge University Press

From the definition $V_\rho^0 = \frac{\partial \chi_\rho^0}{\partial t} = a\cos\omega_R t + b\sin\omega_R t$, the following relation is obtained:

$$d\chi_p^0 = a\cos\omega_R t dt + b\ \sin\ \omega_R t dt.$$

The integration of the above equation from 0 to t gives

$$\chi_p^0 = \frac{a}{\omega_R}\sin\omega_R t - \frac{b}{\omega_R}\cos\ \omega_R t + \frac{b}{\omega_R}.$$

With substitution of the χ_ρ^0 into (A6), we have

$$\frac{\partial \vec{V}^0}{\partial t} + \frac{\partial \vec{V}^1}{\partial t} = \frac{\vec{E}_0}{\sqrt{\varepsilon_\perp}R}\sin\omega_R t - \frac{\chi_\rho^0}{R}\frac{\vec{E}_0}{\sqrt{\varepsilon_\perp}R}\sin\omega_R t$$

$$+ \omega_c \vec{V}^0 \times \hat{e}_z + \omega_c \vec{V}^1 \times \hat{e}_z - \nu\vec{V}^0 - \nu\vec{V}^1$$

and the first order is

$$\frac{\partial \vec{V}^1}{\partial t} = -\frac{\chi_\rho^0}{R}\frac{\vec{E}_0}{\sqrt{\varepsilon_\perp}R}\sin\omega_R t + \omega_c \vec{V}^1 \times \hat{e}_z - \nu\vec{V}^1$$

or

$$\frac{\partial \vec{V}^1}{\partial t} = -\frac{a}{\omega_R R}\frac{\vec{E}_0}{\sqrt{\varepsilon_\perp}R}\sin^2\omega_R t$$

$$+\frac{b}{\omega_R R}\frac{\vec{E}_0}{\sqrt{\varepsilon_\perp}R}\sin\omega_R t\cdot\cos\omega_R t - \frac{b}{\omega_R R}$$

$$\frac{\vec{E}_0}{\sqrt{\varepsilon_\perp}R}\sin\omega_R t + \omega_c \vec{V}^1 \times \hat{e}_z - \nu\vec{V}^1. \quad \text{(A 10)}$$

If we take the average value of time on a motion period, the drift velocity $\vec{u}$ will appear as

$$0 = -\frac{a}{\omega_R R}\frac{1}{2}\frac{\vec{E}_0}{\sqrt{\varepsilon_\perp}R} + \omega_c \vec{u} \times \hat{e}_z - \nu\vec{u}. \quad \text{(A 11)}$$

Separating the above in radial and azimuthal directions, we have

$$0 = -\frac{a}{\omega_R}\frac{E_0}{2\sqrt{\varepsilon_\perp}\cdot R^2} + \omega_c u_\theta - \nu u_\rho \quad \text{and} \quad 0 = -\omega_c u_\rho - \nu u_\theta. \quad \text{(A 12)}$$

By solving the (A12) system, the rf gradient drifts are obtained as

$$u_\theta = -\frac{\omega_c}{\nu^2+\omega_c^2}\cdot\frac{a}{\omega_R}\frac{E_0}{2\sqrt{\varepsilon_\perp}\cdot R^2} \quad \text{and}\ u_\rho = -\frac{\nu}{\omega_c}u_\theta. \quad \text{(A 13)}$$

If a is taken from E(A9) and $\varepsilon_\perp$from (A4), the azimuthal drift is obtained as

$$u_\theta = -\frac{\omega_c}{\omega_c^2+\nu^2}\frac{E_0^2}{2R^3}\frac{\omega_c^2-\nu^2-\omega_R^2}{(\omega_R^2-\nu^2-\omega_c^2)^2+4\nu^2\omega_R^2-\omega_p^2(\omega_R^2+\nu^2-\omega_c^2)}. \quad \text{(A 14)}$$

References

Arzimovich, L. A. 1965 *Elementary Plasma Physics*. New York: Braisdell.

Block, D., Piel, A., Schröder, C. H. and Klinger, T. 2001 *Phys. Rev. E* **63**, 056401.

Chen, F. 1964 *Phys. Fluids* **7**, 949–955.

D'Angelo, N. 1963 *Phys. Fluids* **6**, 592–593.

D'Angelo, N. and Motley, R. 1963 *Phys. Fluids* **6**, 422–425.

Drummond, J. 1961 *Plasma Physics*. New York: Mc Graw-Hill.

Ellis, R., Marden-Marshall, E. and Majeski, R. 1980 *Plasma Phys.* **22**, 113–132.

Heald, M. A. and Wharton, C. B. 1965 *Plasma Diagnostics with Microwaves*. New York: John Wiley, p. 30.

Hendel, H. W., Coppi, B., Perkins, F. and Politzer, P. A. 1967 *Phys. Rev. Lett.* **18**, 439–442.

Klinger, T. 1998 Control of chaos in plasmas. In: *Handbook of Chaos Control* (ed. H. G. Schuster). Weinheim: Wiley-VCH, ch. 20, pp. 513–562.

Koepke, M. E., Klinger, T., Seddighi, F. and Piel, A. 1996 *Phys. Plasmas* **3**, 4421–4426.

Krall, N. and Trivelpiece, A. 1973 *Principles of Plasma Physics*. Tokyo: McGraw-Hill Kogakusha.

Lakhina, G. S. and Shukla, P. K. 1987 *Astrophys. Space Science* **139**, 275–279.

Lieberman, M. and Lichtenberg, A. 1994 *Principles of Plasma Discharges and Materials Processing*. New York: John Wiley.

Marden-Marshall, E., Ellis, R. F. and Walsh, J. E. 1986 *Plasma Phys.* **28**, 1461–1482.

Moreno, T. H. 1948 *Microwave Transmission Design Data*. New York: Dover, p. 66.

Shukla, P. K., Birk, G. and Bingham, R. 1995 *Geophys. Res. Lett.* **22**, 671–674.

Spitzer, L. 1967 *Physics of Fully Ionized Gases*, 2nd edn. New York: John Wiley.

Vranjes, J., Saleem, H. and Poedts, S. 2004 *Phys. Rev. E* **69**, 056404.

Wesson, J. 1997 *Tokamaks*, 2nd edn. Oxford: Clarendon Press.

Xaplanteris, C. L. 1987 *Astrophys. Space Science* **139**, 233–242.

Xaplanteris, C. L. 2009 *J. Plasma Phys.* **75**, 395–406.

Xaplanteris, C. L. 2011 *J. Plasma Phys.* **77**, 15–29.

Xaplanteris, C. L. and Filippaki, E. 2011 *J. Plasma Phys.* 77, 679–692.

https://doi.org/10.1017/S0022377811000535 Published online by Cambridge University Press